DOR: 20.1001.1.27170314.2022.11.3.1.1

Research Paper

Investigation of Effective Parameters on the Surface Temperature Gradient under Equal Channel Angular Pressing Process of AA2017

Fasrhid Ahmadi[1*], Hadi Mansouri[1], Elyas Sarami Foroushani[2]
[1]Department of Mechanical Engineering, University of Kashan, Kashan 8731753153, Iran
[2]Department of Mechanical Engineering, Najafabad Branch, Islamic Azad University, Najafabad, Iran
[*]Email of Corresponding Author: fa.ahmadi@kashanu.ac.ir
Received: July 10, 2022; Accepted: September 23, 2022

Abstract
In recent years, processes known as severe plastic deformation (SPD) have been devised to create fine-grained materials. Among these processes, equal channel angular pressing (ECAP) has been more favored than other methods due to its high efficiency, simplicity, and industrial production potential. This study aimed to investigate the sample temperature gradient during the ECAP process. For this purpose, a Taguchi experiment with influencing factors on AA2017 alloy was designed and a relationship was obtained to predict sample surface temperature. Experiments were carried out using grease, graphite powder, and MoS_2 lubricants, along with routes A, B_C, B_A, and C. The surface temperature of the sample was measured using a laser thermometer. A finite element model was compared with the experimental conditions, and the simulation and experimental results of surface temperature were verified with an error of about 1.9%. In experiments, it was found that speed and lubricant had a significant effect on sample temperature during the process. The simulation results showed that decreasing the die angle resulted in a significant increase in temperature. Following the validation of the FEM model, the temperature gradient and distribution in the middle of the sample, wherein practical experiments could not be measured, were also investigated.

Keywords
Severe Plastic Deformation, Equal Channel Angular Pressing, AA2017 Alloy, Temperature Gradient

1. Introduction

The ECAP process, which is a suitable method for generating large plastic strains, was invented in the early 1990s by Segal et al [1]. The main objective of this method is to introduce a deformation method for high (shear) plastic strains in the material. This process is currently considered the most advanced method of SPD processes. In this method, a uniform sample passes through the plane of two angular intersecting channels with equal dimensions, which results in the application of shear strain to the sample. The sample shape remains constant; therefore, repeated pressures cause large strains. The advantages of this method are tool design and fabrication simplicity, low-cost operation, and proper performance [2]. Different types of ECAP routes such as rotating the sample around the pressure axis between successive passes lead to different microstructure and texture results [3, 4].

Figure 1 schematically illustrates the ECAP process. As shown in the figure, Φ is the channel bending angle. There is also another angle called ψ that shows the curvature at the intersection of two channels. A sample of channel size is compressed by the punch into the die.
The basic principles of this process such as extrusion mechanism, extraction of optimum process conditions, tool geometry, strain path, and their influence on microstructure have been formulated in preliminary papers on this process by Segal [6-9].

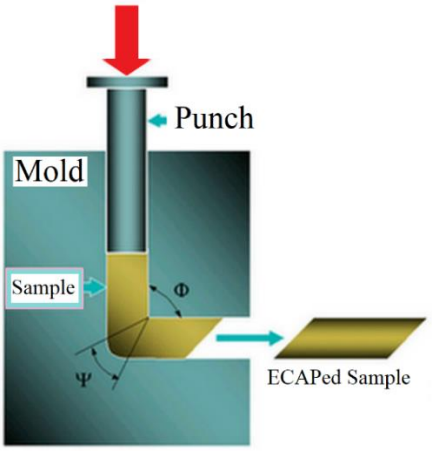

Figure 1. Schematic Overview of the ECAP process [5]

Four different routes of ECAP are schematically shown in Figure 2. In route A, the sample presses again into the die without any rotation. In route B_A, the sample rotates 90 degrees in various directions between successive passes. In route B_C, the sample rotates 90 degrees in a direction (clockwise or counterclockwise) between consecutive passes. In route C, the sample rotates 180 degrees after each pass. Using different routes along with different numbers of passes through the die can lead to the variation of microstructure orientations as well as the creation of a uniform texture. Experiments show that among these paths, the B_C is the most rapid way to reach the high-angle grain boundary materials [10-13]. Increasing the efficiency of the process in the production of finer grains along with more homogeneity of the obtained microstructure has been the main goal of researchers in this field [14-17].

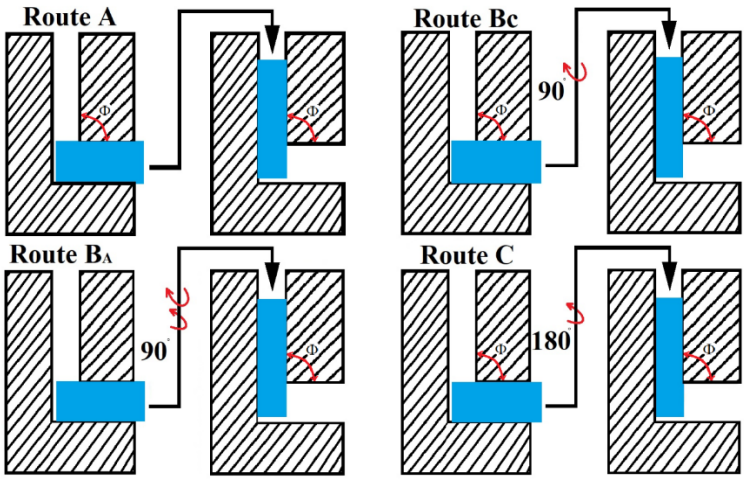

Figure 2. Routes in the ECAP process [18]

The deformation temperature also plays an important role in the ECAP process. During plastic deformation, the sample temperature increases as a result of the heat generated by mechanical work. Equation (1) shows that the mechanical energy per unit volume (w) used for the deformation is equal to the area under the stress-strain curve.

$$W = \int_0^{\bar{\varepsilon}} \bar{\sigma} d\bar{\varepsilon} \qquad (1)$$

Where $\bar{\sigma}$ is the effective stress and $\bar{\varepsilon}$ is the effective strain.

Only a small portion of this energy (mainly in the form of dislocations and atomic vacancies) is stored. This part decreases from the initial value of 5% to 1-2% at high strains. The rest of the energy is released as generated heat. In adiabatic deformations, the temperature rise is obtained from the relation (2):

$$\Delta T = \frac{\alpha \int \bar{\sigma} d\bar{\varepsilon}}{\rho C} = \frac{\alpha\, \bar{\sigma}_a\, \bar{\varepsilon}}{\rho C} \qquad (2)$$

Where $\bar{\sigma}_a$ is the average stress value in the strain interval of zero to ε, ρ is the density, C is the mass heat capacity and α is the fraction of stored energy (0.98).

In recent years, sample temperature gradient during the process has been simulated, but little effort has been made to investigate this issue in experimental situations. In 2016, Guo et al. simulated the deformation temperature changes for pure copper and compared them with experimental results. They demonstrated that the initial state of the material had a significant effect on its temperature gradient during the process [19]. In 2015, Biswas et al. studied the role of the deformation temperature in the structure after the ECAP process and found that excessive temperature increases during deformation could destroy the structure uniformity after ECAP [20].

Valiev et al. in 2014 investigated the effect of back pressure on the ECAP process at high temperatures and stated that temperature rising during the process can affect the results [2].

Also, ECAP simulation has been investigated in some papers for generated heat of Ti-6Al-4V [21], the temperature rise of the AZ31 [22], the effect of initial process temperature on temperature rise and heat distribution of Cp-Ti sample [23], temperature changes and its distribution of Al-Mg alloys [24], the effect of superimposing ultrasonic vibration on the punch [25], and proposing a new route for ECAP [18].

It has been observed that little experimental effort has been made so far to investigate the sample temperature gradient during the ECAP process. To achieve the best results, the design of the die should be proper and process conditions must perfectly be controlled. Several factors can influence the final result, like molding situation, sample size, process speed, and sample temperature during the process. During the process, the sample temperature increases due to the presence of friction and the deformation process. Excessive temperature rise can lead to recrystallization and an increase in grain size, which ultimately creates inaccurate results. Therefore, it is important to investigate the factors affecting temperature [5]. In this research, the effect of speed, lubricant, sample length, and process route was compared using experimental and simulation results.

2. Experimental procedure

AA 2017 alloy was applied in the current study. Samples were prepared with a diameter of 20mm and length of 40, 50, and 60mm. Samples were annealed for 3 hours at 415°C and returned to the

ambient temperature in the furnace to make the structure softer and more uniform. Table 1 shows the chemical composition of the used alloy.

Reducing the effective length is one of the ECAP process characteristics. In other words, after the process, due to sample bending in the die, both ends change their primary cylindrical shape. Figure 3 shows the sample before and after the process.

Table 1: The chemical composition of elements in terms of wt%

Al	Si	Fe	Cu	Mg	Zn	Ni	Cr	Pb	Ti	Be	Mn
Bal.	0.258	0.418	3.59	0.51	0.023	0.011	0.082	0.005	0.014	<0.001	0.96
Ca	Sr	Bi	V	Zr	Sn	Na	B	Ag	P	Co	Li
0.001	<0.001	<0.001	0.004	0.001	0.007	0.001	0.004	0.001	0.006	<0.001	0.068

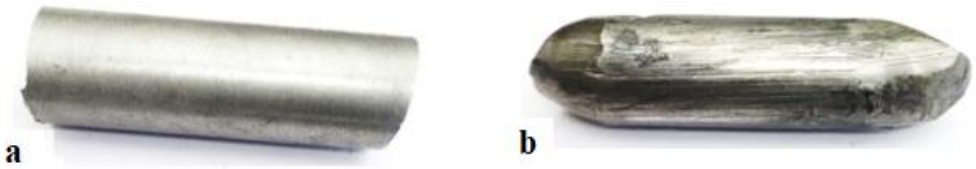

Figure 3. Sample, a) Before the process, b) After four passes of the ECAP

For this study, a die with a diameter of 20 mm, $\Phi = 120$ °, and $\psi = 20$ ° was designed. Figure 4 shows the assembled setup along with the 3D drawing of the die.

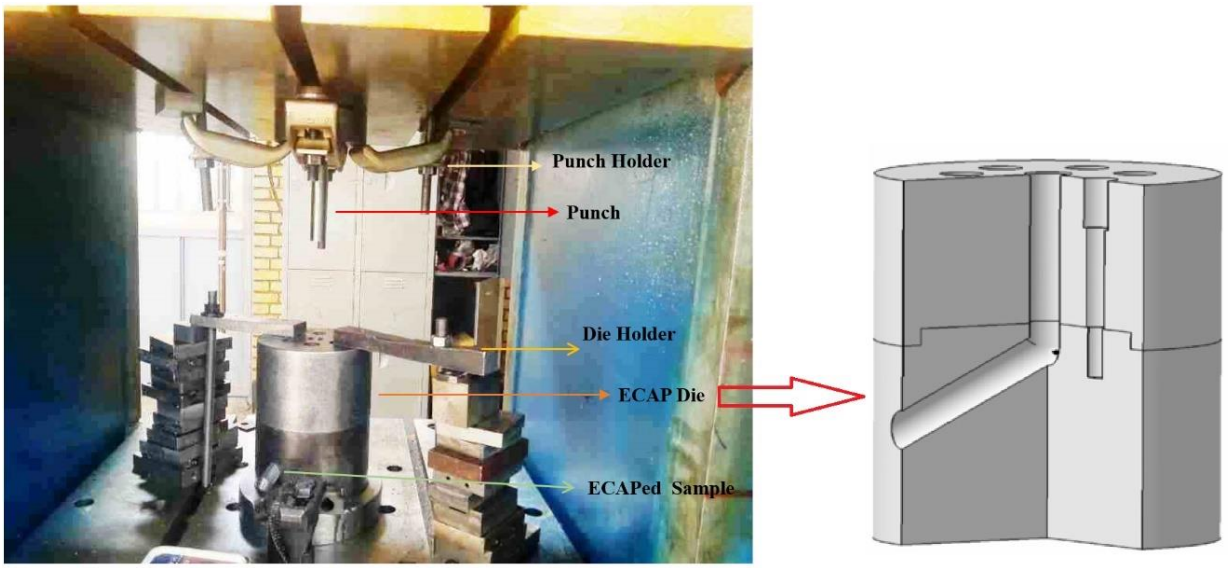

Figure 4. Assembled molding for the experiment

Heat-resistant grease, graphite powder, and MoS_2 were used for lubrication. Graphite and MoS_2 were mixed with lubricating oil and samples were lubricated before the operation. According to Figure 5, a Raytek MX2 laser thermometer with a working range of -30 to 900 °C was used to measure the samples' temperature before and after deformation.

The initial temperature of all samples was in the range of 30 °C. Each experiment was performed with two samples and the mean value was considered the true result.

Figure 5. Raytek MX2 laser thermometer

3. Finite element simulation

In this study, the ECAP process was also simulated for one pass with Abaqus software, to compare the simulation and experimental results. FEM simulation helps to investigate the process where experimental tests are not possible as well as to study the temperature distribution inside the material. To reduce the computation volume, the punch and die were modeled as discrete rigid and the samples were modeled as 3D deformable solid. It should be noted that due to the symmetry of the system, the simulation was performed in the form of plane symmetry. The features required to solve this simulation are presented in Table 2. In this simulation, the Johnson-Cook model was used to define the plastic properties. Johnson-Cook structural and strain failure models are expressed in equations (3) and (4), respectively [26-28].

$$\sigma = [A + B\varepsilon^{n}][1 + C \ln \dot{\varepsilon}^{*}]\,[1 - T^{*m}] \quad (3)$$

$$T^{*} = \frac{T - T_0}{T_m - T_0} \quad (4)$$

In the above relation, ε is the applied strain to the sample, $\dot{\varepsilon}^{*}$ is unit-free plastic strain rate which proves $\frac{\dot{\varepsilon}}{\dot{\varepsilon}_0}$ where $\dot{\varepsilon}_0 = 1.0\mathrm{s}^{-1}$. T^{*} is the equilibrium temperature, T_0 is the ambient temperature, T_m is the melting temperature, A, B, C, m, and n are the five constants that are obtained experimentally at $T^{*} = 0$ and $\dot{\varepsilon}^{*} = 1$ [29, 30]. Table 2 also presents the Johnson-Cook relation parameters and other features used in the simulation. In the heat properties of the material, the inelastic heat fraction is considered to be 0.9. In this simulation process speed, friction coefficient, and die angle parameters were investigated and other parameters were assumed constant for all situations. By performing several simulations and comparing them with the experimental results the best simulation was designed. In each simulation, only the parameter that was intended to evaluate its effect was changed and all other parameters were kept constant. Then, the effect of each parameter on temperature changes was investigated.

To have a precise study, three points on the surface, shown in Figure 6-a, and at the lower part of the sample were selected to study the temperature changes. Point 1, in contact with the corner radius of the die, point 2 in contact with the sharp edge of the die, and point 3, between the other two points on the outer surface, were selected. According to Figure 6-b, three paths were defined on the sample.

Figure 6-b shows the zero point of each path and the maximum path length with the letters "a" and "b", respectively. Diagrams are plotted in these directions.

Table 2. Characteristics of the simulated material [26-28, 31]

Parameter	Value	Parameter	Value
Density	2790 kg/m^3	Elastic Modulus	74.2 GPa
Yield Strength	68.9 MPa	Poisson's Ratio	0.33
Ultimate Tensile Strength	179 MPa	Elongation on Fracture	22%
Heat Transfer Coefficient	193 W/m.K	Specific Heat Capacity	880 J/kg°C
A	53.68	B	116.32
C	0.0234	M	0.78
n	0.266	T_m	893

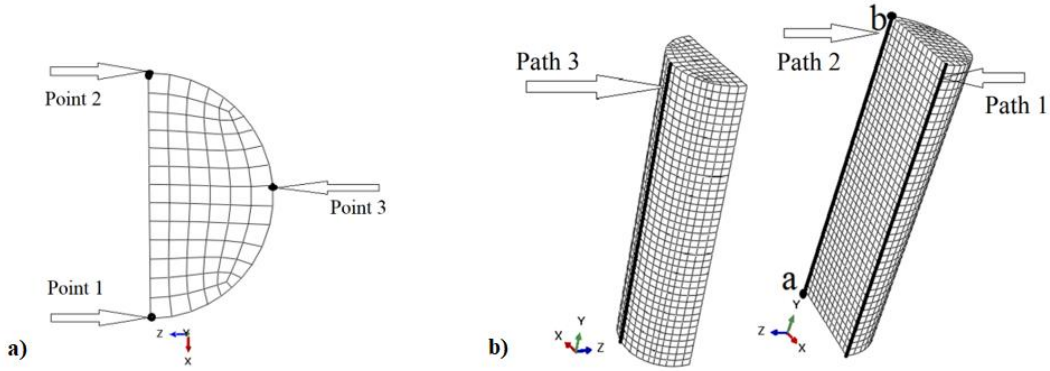

Figure 6. a) Selected points on the sample surface b) Sample analyzing paths

4. Results and discussion

4.1. Experimental results

To increase accuracy, each experiment was performed on two samples, and the mean value of the results was considered. Then, the results of the experiments and the effect of process speed, sample length, lubricant, and process route parameters were investigated. The type of the route was also investigated to observe the effect of this parameter on the temperature distribution. After the simulation verification, the results of experiments and simulations were investigated on the temperature distribution at different points. Then, by performing an experimental design, the factors affecting the process were statistically analyzed and correlated for temperature estimation.

Experiments were performed by changing only one factor and keeping the other factors constant. Table 4 summarizes the conditions of the practical experiments. The results of the experiments were very close to each other due to the low speed of the experiments (limitations of the press), therefore, to increase the accuracy of each experiment, two samples were performed, and the mean value of the results was considered.

Four parameters of speed, lubricant, sample length, and process route were assumed to be variable during the experiments, and others were assumed constant (Table 3). Thus, Samples were deformed four times for each process step.

Table 3. General Conditions of Experiments

Sample	Speed	Lubricant	Length	Route
1	2	MoS_2	60	B_c
2	1.5	MoS_2	60	B_c
3	0.5	MoS_2	60	B_c
4	2	Grease	60	B_c
5	2	Graphite	60	B_c
6	2	MoS_2	60	B_c
7	1.25	MoS_2	40	B_c
8	1.25	MoS_2	50	B_c
9	1.25	MoS_2	60	B_c
10	2	MoS_2	60	A
11	2	MoS_2	60	B_a
12	2	MoS_2	60	B_c
13	2	MoS_2	60	C

To investigate the effect of the processing speed, three tests were performed with different speeds of 2, 1.25, and 0.5 mm/s for a sample with a length of 60 mm and under the conditions of MoS_2 lubrication. Route Bc was used in the tests and the results of each pass are shown in Figure 7-a. The figure proves, increasing the speed increases the sample temperature too. This may be due to the higher heat produced in the material at higher speeds during deformation. Also, increasing the processing speed reduces the heat transferring time from sample to environment and ultimately increases the final temperature of the sample.

Figure 7-b shows the results of experiments with different lubricants. For experiments, the processing speed was 2 mm/s and Route Bc was considered for different passes. The experiment was repeated three times with graphite powder, which was fractured during all three stages of the sample after the third passage. This may be due to the penetration of the graphite particles into the material for high pressure and crack creation resulting in fracture of the sample, hence, the graphite particles glide and no proper lubrication happens. This indicates that graphite powder does not perform well in reducing the friction coefficient of this process. Grease and MoS_2 powder had approximately identical performance in experiments.

To evaluate the effect of sample length, lengths of 40, 50, and 60 mm were prepared from the sample and the ECAP process was carried out using MoS_2 lubricant and at a speed of 1.25 mm/s. Due to the material flow through the die channel, some curvatures form at both ends of the sample, which are not dependent on the sample length. Therefore, increasing the sample length leads to an increase in the useful length after the process and it is necessary to study the effect of this factor on temperature changes.

According to Figure 7-c, sample length has a negligible effect on temperature changes. However, the temperature values of shorter samples are lower than longer samples. Since the shorter samples stay longer in the die, they have more time to transfer their temperature to the die. The sample with 40mm length had a lower temperature at the time of exiting than other samples and its temperature was almost constant during four passes. It can be concluded that the heat generated in this sample is equal to the heat transferred to the environment during the process under the same conditions.

One of the most influential parameters of the ECAP process is the process route. By performing 4 tests on 60 mm samples, at a processing speed of 2 mm/s and using MoS_2 lubrication, the effect of different routes is investigated. According to Figure 7-d, the performances of three routes B_A, B_C,

and C are approximately similar. However, after four successive passes, the temperature of the sample in route BC was slightly lower than the other three samples. The temperature was measured in the part of the sample in contact with the sharp edge of the die. In route A, a slight decrease in temperature was observed. It can be concluded that route A does not affect the proper temperature distribution.

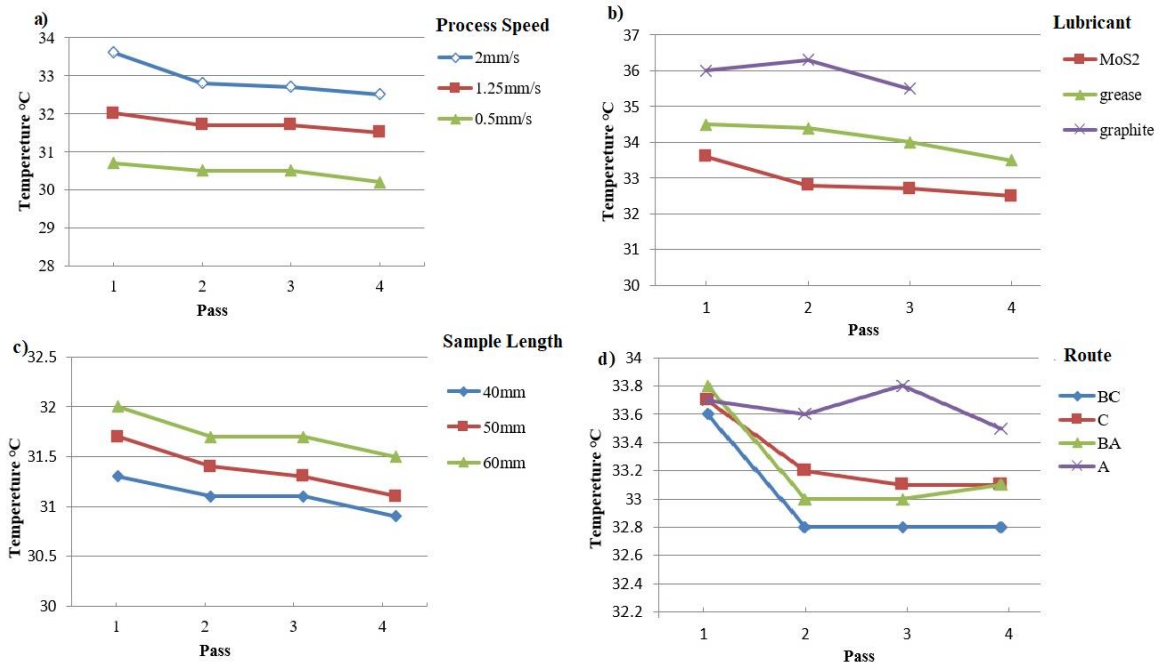

Figure 7. Temperature gradient by changing (a) speed, (b) lubricant, (c) sample length, (d) process route after four passes

The results presented above also show the effect of passing numbers on sample temperature. In all cases, the sample temperature was higher after the first pass rather than during the other passes. Considering the decrease in temperature, it can be concluded that the heat transferred to the environment in subsequent passes is higher than the heat generated in the sample. It should be noted that increasing the processing speed, increases the sample temperature and decreases the temperature transferring time.

4.2. Simulation results

The simulation conditions should be as similar as possible to the experimental conditions, to evaluate the effect of mentioned factors and compare them together. In experiments at low speeds, it was observed that changing the sample length had little effect on temperature changes. Therefore, to reduce the time and volume of the problem, simulations with a sample length of 40 mm, a friction coefficient of 0.1, and process speeds of 0.5, 1.25, and 2 mm/s (according to experiments) were performed. In simulations $\Phi = 120°$ and $\psi = 20°$ were considered. Figure 8 shows the experimental and simulation results of path 2 (according to Figure 6) on the sample temperature. The maximum error between the two curves can be seen at the speed of 0.5 mm/s, which is about 1.9%.

Four higher speeds, which could not be performed experimentally, were also investigated. Figure 9 shows the maximum sample temperature in simulations with speeds of 10, 18, 23, and 30 mm/s. It can be seen that speed increasing rises the temperature but the slope of the curve decreases. So as a result, at very high speeds the effect of speed decreases. Based on the simulation and experimental

results, it can be concluded that speed increasing, rises the sample temperature. At low speeds, the temperature diagram changes linearly with the processing speed.

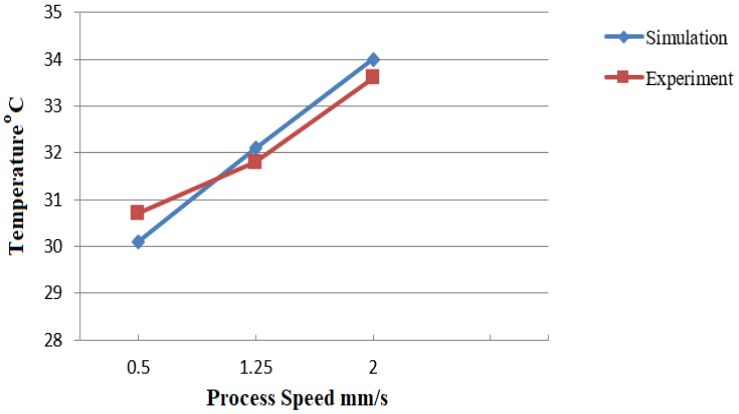

Figure 8. Simulation and experimental results of sample temperature changes with the process speed

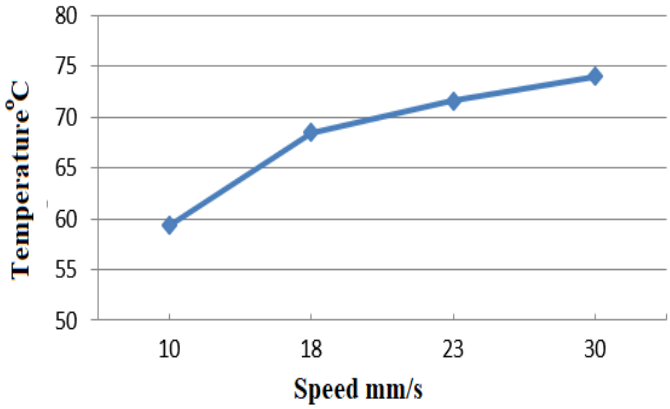

Figure 9. Effect of speed on temperature changes in simulation

To investigate the effect of speed on the temperature distribution of the sample, the graphs of the final temperature distribution on path 3 specified in Figure 6 can be seen in Figure 10. In this diagram, the temperature of the sample is expressed in Kelvin. Figure 10 shows the sample temperature rise due to the increase in speed. The distribution of temperature on the other two paths doesn't vary much at different speeds. The temperature distribution for the speed of 0.5 mm/s is more uniform rather than the other two speeds, and the temperature along the sample can be assumed to be approximately constant. This may be due to the longer process time during which the heat generated is transferred to other parts of the sample, resulting in a more uniform temperature distribution.

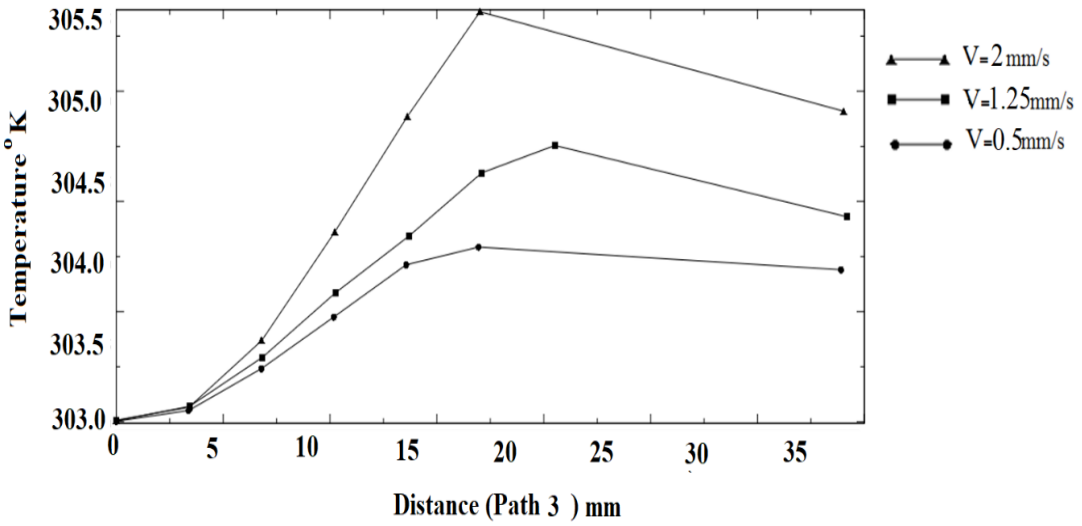

Figure 10. Temperature variations with speed on path 3

In all curves, the maximum temperature is related to the parts of the sample which is deformed. After this section, all curves fall, indicating low temperature at the bottom of the sample. The undeformed section has a lower temperature, and a slight increase in temperature at the beginning of the process is due to the frictional heat and the heat transferred from other parts. Temperature variation is more at speed of 2 mm/s, due to the lower process time for the temperature to transfer from other sections of the sample. In Figure 11, temperature curves are shown for speeds of 10, 18, 24, and 30 mm/s on path 3.

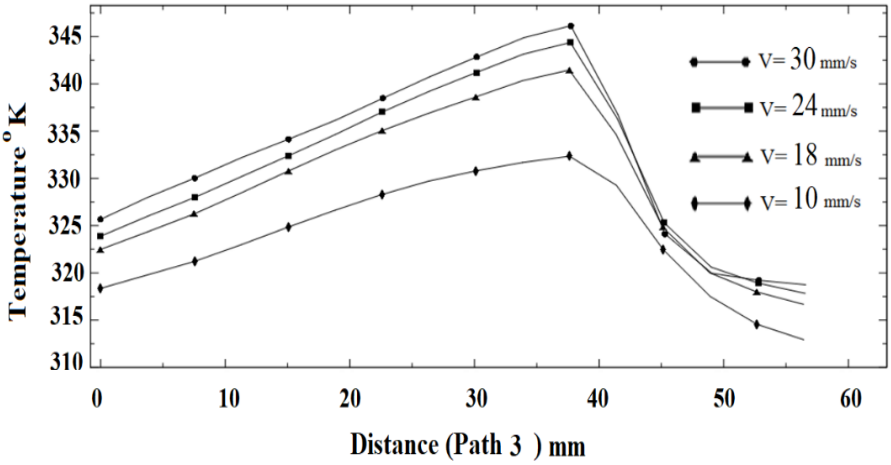

Figure 11. Temperature variations with speed on path 3

The general shape of the diagrams obtained from the simulation at low and high speeds are similar. Their main difference is at higher temperatures. Due to the reduced process time, the heat does not have enough time to move along the sample, which increases the slope of the ascending and descending sections of the graph.

In experimental tests, a lubricant is used to reduce friction, and in simulations, the friction coefficient is selected based on the results of previous studies. To investigate this parameter, the simulation was performed at a speed of 18 mm/s, a sample length of 60 mm, and friction coefficients of 0, 0.05, 0.1, and 0.2 and in a die with conditions of $\Phi = 120\ °$ and $\psi = 20\ °$. The results of the maximum reported

temperature is given in Figure 12. As expected, increasing the friction coefficient increases the temperature.

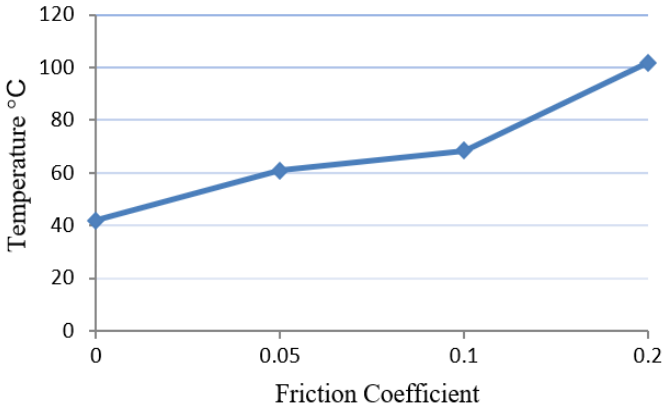

Figure 12. Graph of temperature changes with increasing friction in the simulation

The graph of the sample temperature changes during the process was extracted for all three points specified in Figure 6. However, due to the same trend of graphs for all three points, these changes are shown only for point 2 in Figure 13.

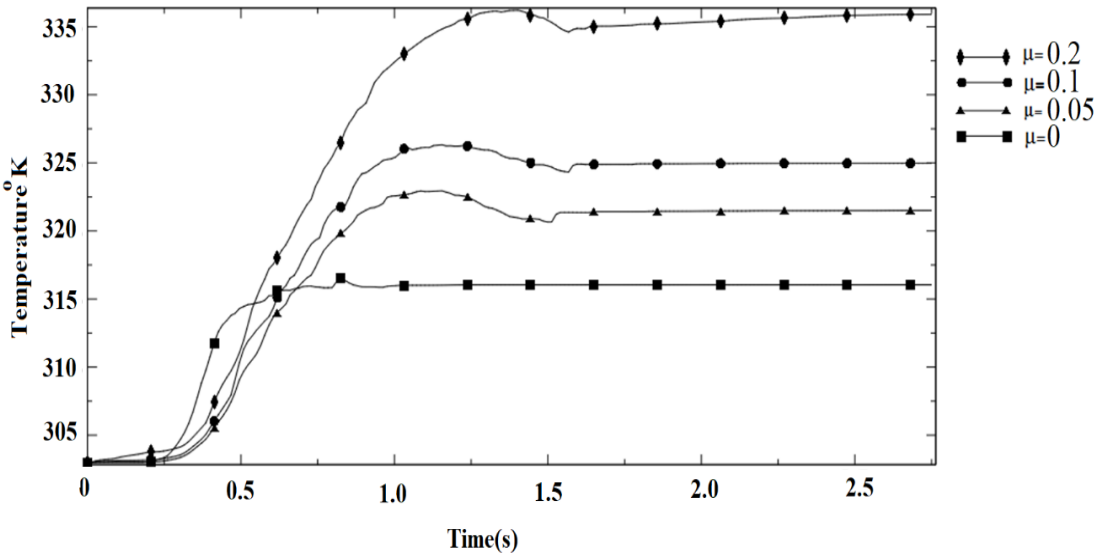

Figure 13. Temperature variations on point 3, V = 18 mm/s, Φ = 120, L = 60 mm

It is seen that the temperature rise is directly related to the friction coefficient. In all graphs the temperature fixes after passing the shear plane. This indicates that the frictional heat generated is equal to the heat transmitted between different sections. The duration of temperature rise in the sample increases with increasing friction coefficient. In other words, the simulation temperature increases with a friction coefficient of 0.2 until the end of the process, but at lower friction coefficients the temperature rise stops earlier.

Figure 14 shows the temperature gradient for simulation with a friction coefficient of 0.1 at all three points. Temperature increase at point 1 starts earlier and is greater than the other two points. Because this point enters the bending plane of the channel earlier, the die friction increases its temperature before other points. Since point 2 has no contact with the die during deformation, its temperature rise

is less than other points. It can be concluded that sample rotation between passes distributes the temperature, uniformly.

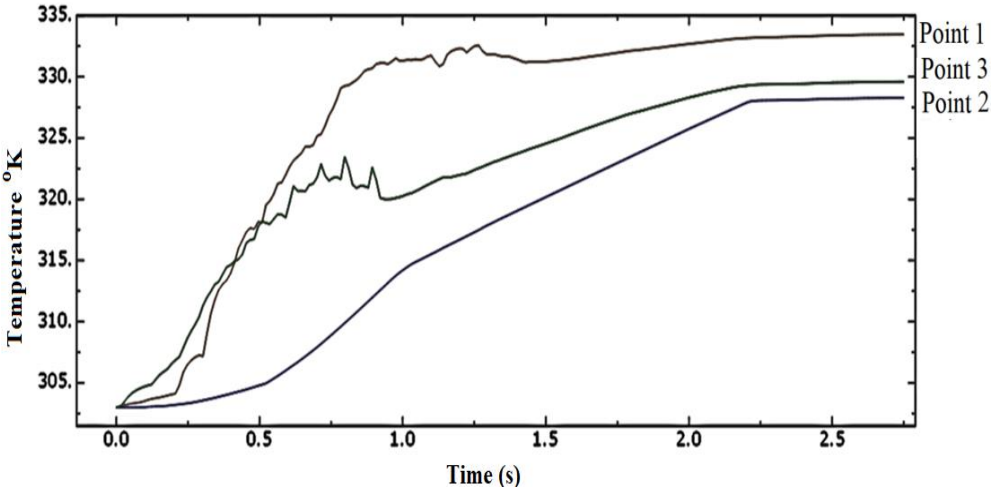

Figure 14. Temperature gradient during the process for all three points in the simulation with the friction coefficient of 0.1

As the die angle increases, the amount of applied strain to the sample decreases [10]. The sample temperature rise is also expected to reduce as the die angle increases. This factor was investigated by performing four simulations with a sample length of 60 mm, a friction coefficient of 0.1, and a processing speed of 18 mm/s. In these simulations, dies with angles of 90, 105, 120, and 135 degrees were designed with a ψ angle of 20 degrees. Figure 15 shows the results of maximum sample temperature in these simulations. As can be seen, increasing the die angle decreases the amount of final sample temperature linearly.

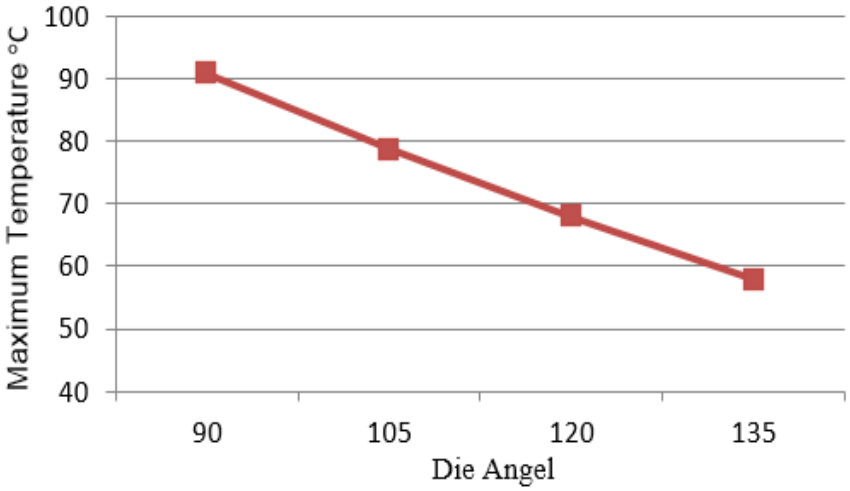

Figure 15. Effect of die angle on temperature distribution

Figure 16 presents that decrease in the die angle results in an increase in the final temperature for point 1. Comparing all four diagrams of each point shows that the temperature rise at point 1 is greater than at the other two points. At all three points, the sample temperature remains constant after crossing the shear plane.

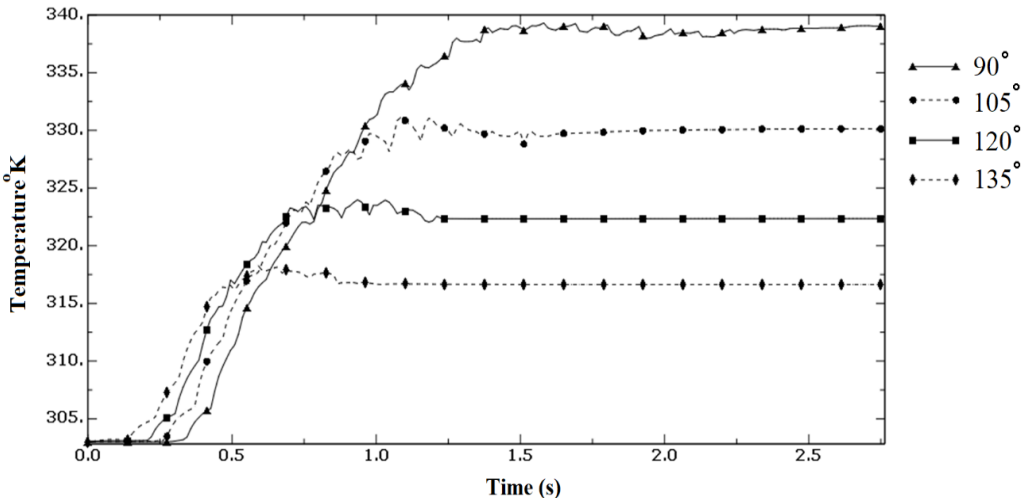

Figure 16. Temperature gradient on various die angle at point 1 V = 18 mm/s, Φ = 120, L = 60 60mm

The obtained contours and diagrams of the simulation are used to study temperature distribution over the surface and volume of the samples. The simulation results showed that the overall temperature distribution in all samples was almost similar. It can be concluded that plastic deformation is the most important factor in the final temperature distribution. In the following, the results of experiments and simulations of the effect of three parameters were statistically analyzed. According to Table 4, three parameters of die angle, friction coefficient, and process speed were determined at four levels for statistical analysis of their effect on sample temperature. The sample length parameter was also eliminated due to its small effect on temperature changes. To investigate these parameters, using the Taguchi method in Minitab software, 16 experiments were designed and simulated. The proposed test scheme and the result of the maximum sample temperature in the simulation are presented in Table 5. It should be noted that other simulation parameters were assumed to be constant.

Table 4. Specified parameters and their levels

Level	Φ	μ	Speed (mm/s)
1	90	0.05	5
2	105	0.1	15
3	120	0.15	25
4	135	0.2	35

After performing the simulations and transferring the results of 16 tests, multivariate regression analysis was performed and the effect of parameters was extracted as a graph. Figure 17 shows the obtained diagrams, in which horizontal and vertical axes show the parameter size and the temperature, respectively. These diagrams are quite similar to those obtained from simulations and experiments. Statistical analysis uses a P-Value to validate the results. The closer this value is to 0, the fewer random data will affect the results. Table 6 shows the P values which are less than 0.05 for all three cases, indicating a high influence of these factors on sample temperature.

Table 5. Test scheme and simulation results of maximum temperature

Sample	Φ	μ	V	Maximum Temperature
1	90	0.05	5	52.9
2	90	0.1	15	77.9
3	90	0.15	25	91.1
4	90	0.2	35	122.2
5	105	0.05	15	65.2
6	105	0.1	5	53.3
7	105	0.15	35	90.3
8	105	0.2	25	98.8
9	120	0.05	25	61.5
10	120	0.1	35	68.6
11	120	0.15	5	47.9
12	120	0.2	15	74.4
13	135	0.05	35	54.3
14	135	0.1	25	56.8
15	135	0.15	15	57.5
16	135	0.2	5	46

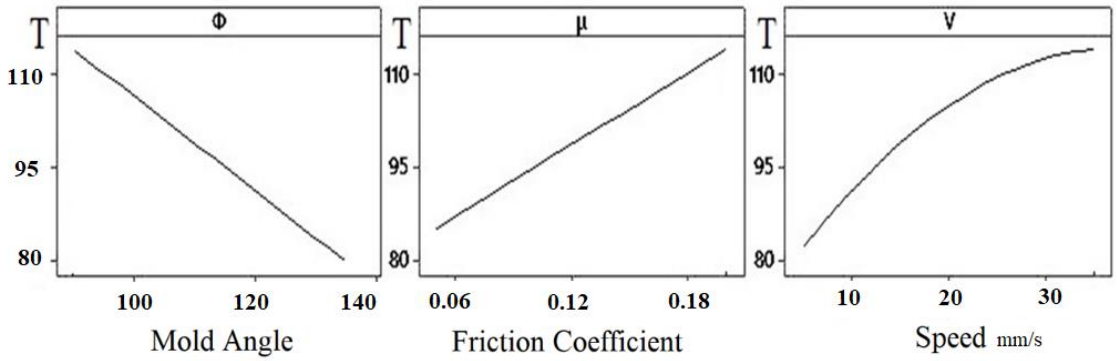

Figure 17. Obtained graphs from the Minitab software

Table 6. P-values for investigated parameters

Parameter	P-value
V	0.04
Φ	0.013
μ	0.044

As shown in Figure 17, increasing the friction coefficient linearly and directly results in an increase in temperature. This figure also shows that increasing the angle of the die channel linearly decreases the final sample temperature. As can be seen, the increase in speed leads to an increase in temperature, but the effect of this factor is reduced at high speeds. Figure 18 shows the interaction of these parameters on the temperature.

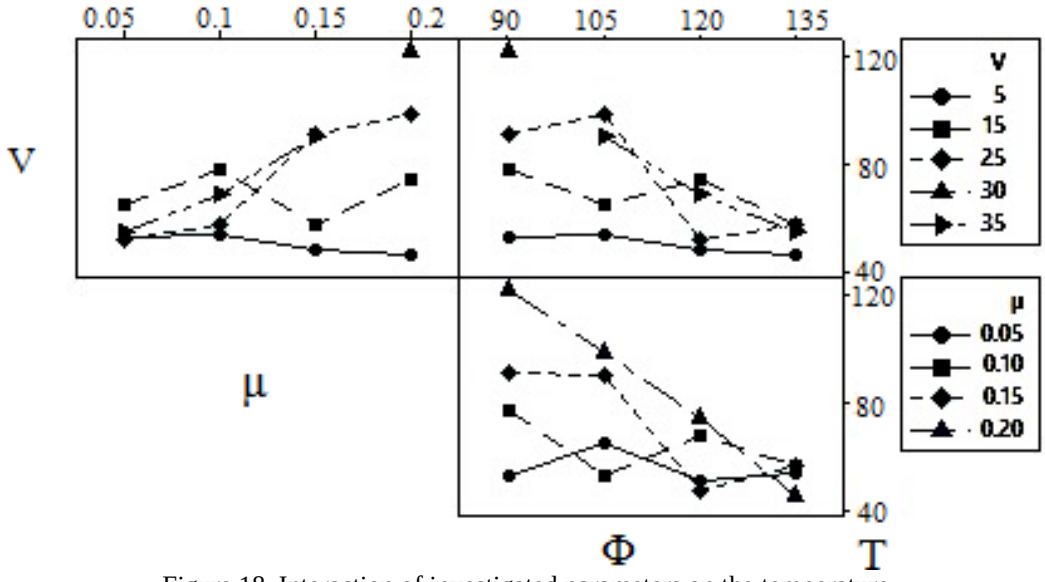

Figure 18. Interaction of investigated parameters on the temperature

From Figure 18, it can be concluded that changing a parameter doesn't change how other factors generally interact, but the following may be noted:

1. The role of process speed is more prominent in high friction coefficients.
2. Effects of all factors on temperature rise greatly reduce at low speeds due to the high process time for heat transfer.
3. The effect of die angle is more prominent at high friction coefficient.

In the current study, Minitab software was used to create multivariate regression analyses to define a relation between input and output parameters for error reduction, and the results were reported as equation 5. Then, the input parameters of tests were placed in equation 5 and calculated results compared to the simulation results and the error value was also obtained (Table 7). Based on the error results, performed statistical analysis can predict the simulation results with proper approximation.

$$T = 101.6 - 0.7638\Phi + 193.6\mu + 2.269V - 0.0302V^2 \qquad (5)$$

To validate equation 5, eight simulations were performed with conditions mentioned in Table 8. Input parameters were again placed in equation 5 and their prediction results were also compared with simulation results and good accordance was obtained which indicates the reliability of this equation for this material. Also given the error of samples 5 to 8, this relation can predict the results of simulations for different lengths. Samples 9 to 11 present the results of three practical experiments with MoS_2 lubrication and their prediction results. The error range is compatible with other samples' results. Therefore, it can be concluded that using the friction coefficient of 0.1 and MoS_2 lubrication, the test can be predicted.

Table 7. Simulation and predicted results

Sample	Simulated maximum temperature	Prediction result	% Error
1	52.9	53.138	0.45
2	77.9	79.458	2
3	91.1	99.748	9.5
4	122.2	113.998	-6.7
5	65.2	58.328	-10.5
6	53.3	51.351	-3.7
7	90.3	92.861	2.8
8	98.8	97.971	-0.8
9	61.5	57.474	11.6
10	68.6	71.724	4.5
11	47.9	49.574	3.5
12	74.4	75.904	2
13	54.3	50.587	-6.8
14	56.8	55.687	-1.9
15	57.5	54.767	-4.8
16	46	47.797	-3.9

Table 8. Conditions of validation Simulations

Sample	Φ	μ	V	L	Simulation	Prediction	% Error
1	105	0.12	20	40	75.4	77.933	3.36
2	120	0.18	10	40	63.5	64.462	1.5
3	90	0.07	8	40	65.6	64.5652	-1.58
4	135	0.16	17	40	59.5	59.3082	-0.32
5	115	0.05	40	70	72.4	65.883	-9.4
6	100	0.1	27	60	89.2	83.8272	-6.02
7	125	0.15	36	50	80.8	77.7098	-3.82
8	125	0.2	13	40	68.7	69.2382	0.78
9	120	0.1	2	60	33.6	33.72	0.35
10	120	0.1	1.25	60	31.8	32.1	0.94
11	120	0.1	0.5	60	30.7	30.4	0.97

4. Conclusion

In this study, the effect of process speed, route, sample length, and lubricant on temperature distribution of AA2017 alloy during the ECAP process was experimentally investigated at ambient temperature. The results are:

1. Process speed has a great effect on temperature rise in such a way that increasing the speed will increase the temperature.
2. Although the process route has a great effect on the microstructure and improves mechanical properties, it does not have a significant effect on the temperature rise of the samples. Different routes can contribute to a more uniform temperature distribution in the sample.
3. The sample length has no significant effect on the final temperature.
4. Proper lubrication can greatly prevent the temperature rise of the specimens. A suitable lubricant must be capable of heat transfer in addition to its ability to lubricate at high pressure. It is not appropriate to use graphite powder lubricant to perform the ECAP process on AA2017 alloy.

5. Using a proper lubricant can reduce the required force. This factor is more prominent in high passes due to the increased strength.

Simulations with input parameters of friction coefficient, process speed, and die angle were performed, and the following results regarding the effect of the mentioned parameters on the temperature rise of the samples were obtained:

1. According to the experimental results, temperature changes have a direct relationship with the processing speed, but at high speeds, its effect is reduced.
2. Increasing the friction coefficient increases the sample temperature.
3. The friction coefficient is the most important factor for surface temperature changes.
4. The die channel angle has a great influence on the sample temperature.

Taguchi method was applied and 16 experiments were designed. Then simulations were performed based on this design and the outputs were analyzed. The following results were obtained:

1. The results of the statistical analysis show the effect of parameters, prominently.
2. The obtained equation by this method can predict the simulation results accurately.

5. References

[1] Segal, V., Reznikov, V., Dobryshevshiy, A. and Kopylov, V. 1981. Plastic working of metals by simple shear. Russian Metallurgy (Metally). 1(1): 99-105.

[2] Valiev R.Z., Zhilyaev, A.P. and Langdon, T.G. 2014. Bulk Nanostructured Materials: Fundamentals and Applications. New Jersey: John Wiley & Sons.

[3] Ferrasse, S., Segal V.M., Alford, F., Kardokus, J. and Strothers S. 2008. Scale up and application of equal-channel angular extrusion for the electronics and aerospace industries. Materials Science and Engineering: A. 493(1): 130-140.

[4] Segal, V.M. 1999. Equal channel angular extrusion: From micromechanics to structure formation. Materials Science and Engineering. A. 271(1): 322-333.

[5] Sklenicka, V., Dvorak, J., Kvapilova, M., Svoboda, M. and Kral, P. 2012. Equal-channel angular pressing and creep in ultrafine-grained aluminium and its alloys. Rijeka: Intech Open Access Publisher,

[6] Segal, V.M., Hartwig, K.T. and Goforth, R. 1997. In situ composites processed by simple shear. Materials Science and Engineering. A. 224(1): 107-115.

[7] Segal, V.M. 1995. Materials processing by simple shear. Materials Science and Engineering: A. 197(2): 157-164.

[8] V.M, Segal. 2002. Severe plastic deformation: Simple shear versus pure shear. Materials Science and Engineering: A. 338(1): 331-344.

[9] Segal, V.M. 2005. Deformation mode and plastic flow in ultra fine grained metals. Materials Science and Engineering: A. 406(1): 205-216.

[10] Suzuki, T., Vinogradov, A. and Hashimoto, S. 2004. Strength enhancement and deformation behavior of gold after equal-channel angular pressing. Materials transactions. 45(7): 2200-2208.

[11] Vinogradov, A., Maruyama, M., Kaneko, Y. and Hashimoto, S. 2012. Effect of dislocation hardening on monotonic and cyclic strength of severely deformed copper. Philosophical Magazine. 92(6): 666-689.

[12] Azushima, A., Kopp, R., Korhonen, A., Yang, D.-Y., Micari, F., Lahoti, G., Groche, P., Yanagimoto, J., Tsuji, N. and Rosochowski, A. 2008. Severe plastic deformation (spd) processes for metals. CIRP annals. 57(2): 716-735.

[13] Mc Nelley, T.R., Swisher, D.L., Horita, Z. and Langdon, T.G. 2002. Influence of processing route on microstructure and grain boundary development during equal-channel angular pressing of pure aluminum. Proceeding of ultra fine grained materials II. Seattle, U.S.

[14] Neshastegir Kashi, A. and Ahmadi, F. 2021. The effect of ECAP die helix angle on the microstructure homogeneity of the processed samples by fem method. Journal of Modern Processes in Manufacturing and Production. 10(2): 27-39.

[15] Shahsavari, M.H. and Ahmadi, F. 2015. Evolution of texture and grain size during equal channel angular extrusion of pure copper and 6012 aluminum. Journal of Modern Processes in Manufacturing and Production. 4(4): 47-58.

[16] Shahsavari, M.H. and Ahmadi, F. 2014. Comparison of hardness values of various specimens with different geometries and material properties after ECAP. Journal of Modern Processes in Manufacturing and Production. 3(3): 61-78.

[17] Sahai, A., Sharma, S.S. and Dwivedi, S.N. 2021. Deformation of al alloy during integrated extrusion and ECAP: A simulation research. Journal of Modern Processes in Manufacturing and Production. 10(3): 35-44.

[18] Ahmadi, F. and Farzin, M. 2014. Investigation of a new route for equal channel angular pressing process using three-dimensional finite element method. Proceedings of the Institution of Mechanical Engineers, Part B: Journal of Engineering Manufacture. 228(7): 765-774.

[19] Guo, T.B., Cao, J., Ding, Y.T. and Jia, Z. 2016. Numerical and experimental study of temperature rise effect on copper during equal channel angular pressing. Materials Science Forum. 850(2): 864-870.

[20] Biswas, S., Brokmeier, H.-G., Fundenberger, J.-J. and Suwas, S. 2015. Role of deformation temperature on the evolution and heterogeneity of texture during equal channel angular pressing of magnesium. Materials Characterization. 102: 98-102.

[21] Miaoquan, L., Zhang, C., Luo, J. and Mingway, F. 2010. Thermomechanical coupling simulation and experimental study in the isothermal ECAP processing of ti-6al-4v alloy. Rare Metals. 29(6): 613-620.

[22] Kim, H.S. 2009. Analysis of thermal behavior during equal channel multi-angular pressing by the 3-dimensional finite volume method. Materials Science and Engineering: A. 503(1): 130-136.

[23] Jiang, H., Fan, Z. and Xie, C. 2009. Finite element analysis of temperature rise in cp–ti during equal channel angular extrusion. Materials Science and Engineering: A. 513: 109-114.

[24] Pei, O., Hu, B.H., Lu, C. and Wang, Y.Y. 2003. A finite element study of the temperature rise during equal channel angular pressing. Scripta Materialia. 49(4): 303-308.

[25] Ahmadi, F. and Farzin, M. 2014. Finite element analysis of ultrasonic-assisted equal channel angular pressing. Proceedings of the Institution of Mechanical Engineers, Part C: Journal of Mechanical Engineering Science. 228(11): 1859-1868.

[26] Johnson, G.R. and Cook, W.H. 1985. Racture characteristics of three metals subjected to various strains, strain rates, temperatures and pressure. Engineering fracture mechanics. 21(1): 31-48.

[27] Johnson, G.R. and Cook, W.H. 1983. A constitutive model and data for metals subjected to large strains, high strain rates and high temperatures. Proceedings of the 7th International Symposium on Ballistics. Netherlands.

[28] Milani, A., Dabboussi, W., Nemes, J.A. and Abeyaratne, R. 2009. An improved multi-objective identification of johnson–cook material parameters. International journal of impact engineering. 36(2): 294-302.

[29] Committee, A. I. H. 2013. ASM Handbook. Volume 4A: steel heat treating fundamentals and processes, Ohio: ASM international.

[30] Sanusi, K.O., Makinde, O.D. and Oliver, G.J. 2012. Equal channel angular pressing technique for the formation of ultra-fine grained structures. South African Journal of Science. 108(9): 1-7.

[31] Committee, A.I.H. 1992. Properties and selection: Nonferrous alloys and special-purpose materials. ASM international, Ohio, U. S.